Synthesis of Convex Hexoctahedral Palladium@Gold Core–Shell Nanocrystals with {431} High-Index Facets with Remarkable Electrochemiluminescence Activities

Ling Zhang,[†,‡] Wenxin Niu,[†,‡] Wenyue Gao,[†,‡] Liming Qi,[†,‡] Jianping Lai,[†,‡] Jianming Zhao,[†,‡] and Guobao Xu[†,*]

[†]State Key Laboratory of Electroanalytical Chemistry, Changchun Institute of Applied Chemistry, Chinese Academy of Sciences, Changchun 130022, China and [‡]The University of Chinese Academy of Sciences, Beijing 100049, China

ABSTRACT Convex hexoctahedral nanocrystals have been synthesized through fast growth kinetics and the use of cetylpyridinium chloride as a capping agent. Monodisperse convex hexoctahedral Pd@Au core–shell nanocrystals with {431} high-index facets are obtained at high reaction rates by using high concentrations of ascorbic acid in the presence of cetylpyridinium chloride. In contrast, octahedral nanocrystals with {111} low-index facets and their {100}-truncated counterparts are formed at low ascorbic acid concentrations. The substitute of cetylpyridinium chloride with cetyltrimethylammonium chloride leads to the generation of concave trisoctahedral Pd@Au core–shell nanocrystals with {331} high-index facets, indicating that cetylpyridinium plays an important role in the formation of convex hexoctahedral nanocrystals. The as-prepared convex hexoctahedral Pd@Au core–shell nanocrystals exhibit remarkable catalytic performances toward electrochemiluminescence compared with truncated octahedral and concave trisoctahedral Pd@Au core–shell nanocrystals.

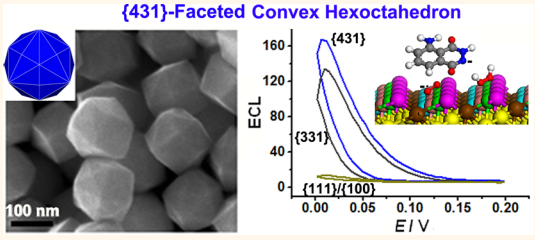

KEYWORDS: crystal growth · high-index facets · gold · convex nanocrystals · electrochemiluminescence · palladium

Noble metals have been extensively utilized as catalysts in organic synthesis, fuel cells, and automobile industry.[1,2] Au and Ag nanocrystals are particularly promising nanoentities able to induce plasmon-induced chiroptical response, surface-enhanced Raman scattering, fluorescence, and electrochemiluminescence enhancement.[1,3,4] The properties of noble metal nanocrystals significantly depend on their structures (*e.g.*, shapes and facets). Nanocrystals with high-index facets have been reported as highly effective catalysts and thus received much attention.[5−11] However, the preparation of high-index-faceted nanocrystals is challenging because the inherent thermodynamic instability of high-index facets makes them disappear during crystal growth.[12] As a result, only a few synthetic methods for concave hexoctahedron (HOH) nanocrystals have been reported,[5,8,13,14] and no chemical reduction method for the synthesis of convex HOH noble metal nanocrystals has been reported to date.

The shapes of colloidal noble metal nanocrystals depend on reaction rates, capping agents, concentrations, temperatures, *etc.*[1,6] The fast growth kinetics may induce the heterogeneous growth of noble metal nanocrystals and the formation of thermodynamically unstable facets due to the quick disappearance of thermodynamically stable facets and/or the supersaturation of metal atoms in the solution under fast reaction rates.[7,15,16] In this study, we develop a facile chemical reduction method to synthesize convex HOH nanocrystals with {431} high-index facets by the combination of fast growth kinetics and the use of cetylpyridinium chloride (CPC) as capping agent. As shown in Scheme 1, convex HOH Pd@Au

* Address correspondence to guobaoxu@ciac.ac.cn.

Received for review February 23, 2014 and accepted May 30, 2014.

Published online May 30, 2014
10.1021/nn501086k

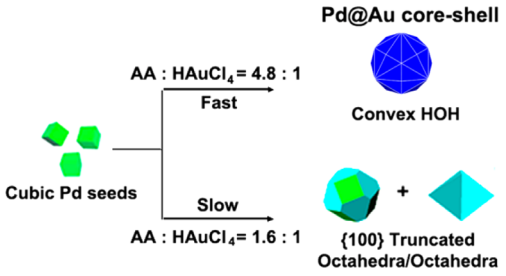

Scheme 1. Growth routes of Pd@Au core–shell nanocrystals.

core–shell nanocrystals are obtained at a high concentration of ascorbic acid (AA) through fast growth kinetics. In contrast, octahedral nanocrystals with {111} low-index facets and their {100}-truncated counterparts (corresponding to the thermodynamic morphologies in Wulff construction) are obtained at low AA concentrations.[17] The convex HOH Pd@Au core–shell nanocrystals exclusively enclosed by {431} high-index facets exhibit remarkably improved electrochemiluminescence (ECL) properties due to the presence of atoms in kink and step sites on {431} high-index facets.

RESULTS AND DISCUSSION

Synthesis of Convex HOH Pd@Au Core–Shell Nanocrystals. In a typical synthesis of convex HOH Pd@Au core–shell nanocrystals, 10 μL of 22 nm cubic Pd seeds (Supporting Information Figure S1) solution and 144 μL of 0.1 M AA solution were added into a growth solution containing 5 mM CPC and 0.6 mM $HAuCl_4$. Figure 1A,B depicts the scanning electron microscopy (SEM) images of the convex HOH Pd@Au nanocrystals. The as-prepared HOH nanocrystals possess excellent shape and size monodispersity. Their sizes are around 156.9 ± 7.2 nm, and the yield is 95.2%. A convex HOH can be seen as a tetrahexahedron with the center of every square edge pulled outward, splitting each $\{h'k'0\}$ facet into two $\{hkl\}$ facets.[1,2,18] To confirm the facets of the HOH nanocrystals, SEM images, transmission electron microscopy (TEM) images, geometric models, and selected area electron diffraction (SAED) patterns of a single HOH nanocrystal projected along the [011], [001], and [$\bar{1}$11] directions are shown in Figure 1C–F, respectively. The relationships between the projected angles of convex HOH along the [011] direction (Figure 1E) and Miller indices (*h*,*k*,*l*) are summarized as follows.

$$\alpha = 2\arctan\left(\frac{\sqrt{2}h}{k+l}\right)$$

$$\beta = 270^\circ - \frac{\alpha+\gamma}{2}$$

$$\gamma = 2\arctan\left(\frac{h+k}{\sqrt{2}l}\right)$$

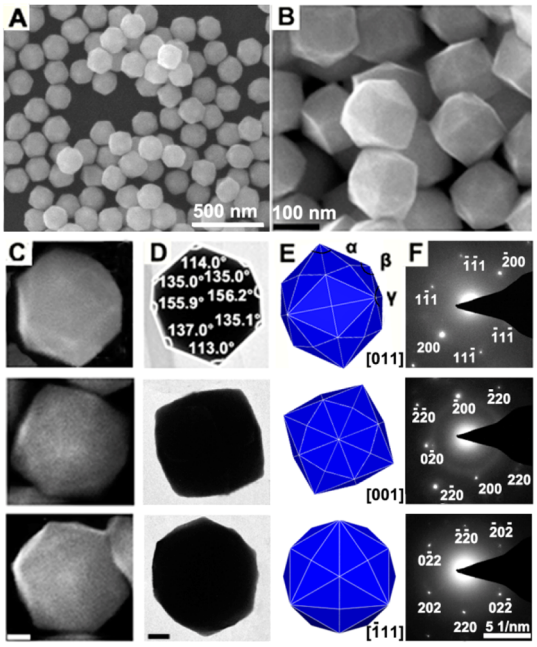

Figure 1. (A) Large-scale and (B) high-resolution SEM images of convex HOH Pd@Au core–shell nanocrystals in the typical synthesis. CPC, 5 mM, AA, 144 μL. (C) SEM images, (D) TEM images, (E) geometric models, and (F) corresponding SAED patterns of a single convex HOH nanocrystal projected along the [011], [001], and [$\bar{1}$11] directions, respectively. Scale bars, 20 nm.

The measured projected angles between the adjacent facets of the polyhedron along the [011] direction (Figure 1D, top image) are 114.0, 135.0, 156.2, 135.1, 113.0, 137.0, 155.9, and 135.0°, respectively, matching well with the theoretical values of {431}-faceted convex HOH nanocrystals (Table S1). These results strongly support the presence of {431} high-index facets on the convex HOH Pd@Au core–shell nanocrystals. When a convex HOH nanocrystal is projected along the [001] direction, the nanocrystal outline approaches a quadrilateral shape with each edge protruding outward, as shown in Figure 1D (middle image). A projection along the [$\bar{1}$11] direction (Figure 1D, bottom image) shows a circle-like feature in the nanocrystal outline due to the abundance of facets, which differs from its concave counterparts having star-like outlines.[1,2]

The sizes of convex HOH Pd@Au core–shell nanocrystals are adjustable by varying the amount of Pd seeds and can affect the extinction spectra of convex HOH Pd@Au core–shell nanocrystals. Figure 2 shows that the sizes of convex HOH Pd@Au core–shell nanocrystals increase as the amount of Pd seeds decreases. The convex HOH Pd@Au core–shell nanocrystals of 60 and 81 nm exhibit surface plasmon resonance (SPR) peaks at 545 and 551 nm (Figure 2D), respectively.[19,20] As the sizes of Pd@Au core–shell nanocrystals increase further, the SPR peaks gradually shift red. Moreover, a broad SPR band in the near-infrared region between 800 and 1000 nm appears when the size of convex HOH Pd@Au core–shell nanocrystals is 157 nm.

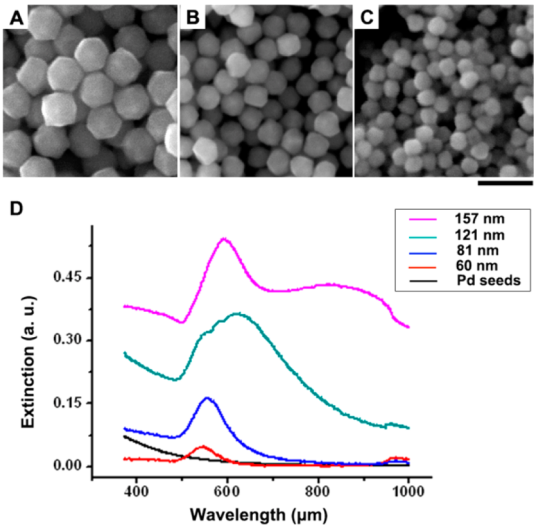

Figure 2. SEM images of convex HOH Pd@Au core–shell nanocrystals with a size of (A) 121, (B) 81, and (C) 60 nm synthesized by adding 50, 100, and 400 μL of Pd seeds into the growth solutions, respectively. Scale bar, 200 nm. (D) Extinction spectra of cubic Pd seeds of 22 nm (the concentration of nanocrystals is 1.5 nM) as well as convex HOH Pd@Au core–shell nanocrystals of 60, 81, 121, and 157 nm (the concentration of nanocrystals is 0.13 nM) dispersed in 5 mM CPC solutions.

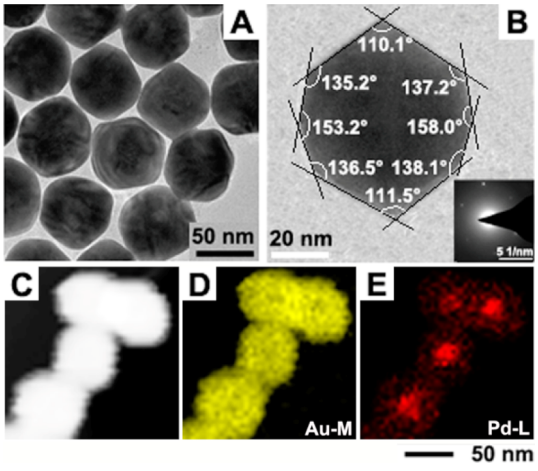

Figure 3. (A) TEM image of convex HOH Pd@Au core–shell nanocrystals of 60 nm. (B) TEM image of a single HOH Pd@Au core–shell nanocrystal oriented along the [011] direction and the corresponding SAED pattern. (C) HAADF-STEM and elemental mapping images for (D) Au and (E) Pd elements.

To confirm the core–shell nanostructure of these convex HOH nanocrystals, the TEM characterization (Figure 3) and X-ray photoelectron spectroscopy (XPS) characterization (Figure S2) of convex HOH Pd@Au nanocrystals of 60 nm have been performed. The measured projection angles in Figure 3B indicate that the convex HOH Pd@Au core–shell nanocrystal of 60 nm is bounded by {431} high-index facets. Figure 3C–E shows the high-angle annular dark-field scanning transmission electron microscopy (HAADF-STEM) and elemental mapping analysis of Au and Pd elements. Au element is distributed around the outer shell, while Pd element is distributed in the center of nanocrystals, confirming the core–shell nanostructure of these convex HOH nanocrystals. Moreover, no peak corresponding to Pd is observed in the XPS spectra (Figure S2).[21,22] It indicates that there is no Pd element on the surface of convex HOH Pd@Au core–shell nanocrystals.

Growth Mechanism of Convex HOH Pd@Au Core–Shell Nanocrystals. For noble metal nanocrystals with face-centered cubic structure, the surface energy of different facets follows the order $\gamma_{\{111\}} < \gamma_{\{100\}} < \gamma_{\{110\}} < \gamma_{\{hkl\}}$.[23] The {110} and {*hkl*} facets are thermodynamically unstable due to the abundance of unsaturated coordinated atoms on their surfaces, consequently denoted as high-energy facets. The high-energy facets usually disappear as crystal growth proceeds. Fortunately, crystal growth is tunable thermodynamically and kinetically.[24] The deposition of Au atoms preferably occurs on the surfaces with many unsaturated coordinated atoms at low reaction rates, facilitating the formation of thermodynamically stable facets such as {111} and {100}. Interestingly, thermodynamically unstable facets can be preserved when the reaction is fast. As shown in Table S2, convex Pd@Au core–shell HOH nanocrystals are only obtained at the high concentrations of reducing reagent in this study, suggesting that fast reduction kinetics plays an important role in the formation of convex HOH nanocrystals. The fast reduction kinetics may also increase the supersaturation of metal atoms in solution, and the excess energy is converted into the surface energy of crystals, leading to the formation of high-energy facets.[7] Slowing down reaction rates by decreasing the mole ratio of AA to $HAuCl_4$ to 1.6:1 results in the formation of {100}-truncated octahedral nanocrystals (Figure 4A), which is the equilibrium morphology with the lowest surface energy predicted by the Wulff theory.[17]

The surface energy of nanocrystals is dependent on temperature, capping agents, solvents, adsorption energy, and so on.[25,26] The capping agent CPC used in this study also affects the surface energy of nanocrystals and the equilibrium shape of Pd@Au core–shell nanocrystals. Some octahedral nanocrystals (Figure 4B) are formed when CPC concentrations increase to 100 mM at a low molar ratio of AA to $HAuCl_4$ (1.6:1). These findings point to a CPC stabilization of the Au {111} facet through selective adsorption on Au surfaces.[20] Importantly, convex HOH nanocrystals (Figure S3) are still obtained even if CPC concentrations increase up to 100 mM at a higher molar ratio of AA to $HAuCl_4$ (4.8:1). The replacement of CPC with cetyltrimethylammonium chloride (CTAC) gave rise to the generation of concave trisoctahedral Pd@Au core–shell nanocrystals with {331} high-index facets (Figures 4C and S4). These results indicate that the pyridinium group of CPC also plays an important role in the formation of convex HOH

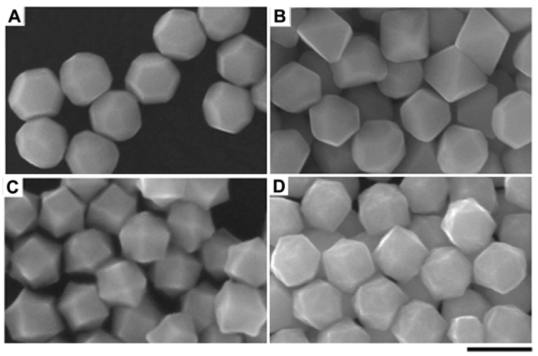

Figure 4. SEM images of (A) truncated octahedral (5 mM CPC + 48 μL AA), (B) truncated octahedral/octahedral (100 mM CPC + 48 μL AA), (C) concave trisoctahedral (5 mM CTAC + 144 μL AA) Pd@Au core–shell nanocrystals, and (D) convex HOH Au nanocrystals synthesized using 39 nm near-spherical Au seeds. Other conditions were the same as those in the typical synthesis. Scale bar, 200 nm.

nanocrystals. If cubic Pd seeds are replaced with near-spherical single-crystalline Au seeds and other conditions are the same as that in the typical synthesis of convex Pd@Au core–shell nanocrystals, the products are still convex HOH nanocrystals with {431} high-index facets, as shown in Figures 4D and S5. It suggests that the formation of {431} facets is possible using different seeds.[27−29] As shown in Figure S6, convex HOH Au nanocrystals can also be formed without adding seeds. The structure and shape of noble metal nanocrystals have some effects on their SPR properties. Figure S7 shows that the extinction peak wavelengths of convex HOH, truncated octahedral, and concave trisoctahedral Pd@Au core–shell nanocrystals, as well as convex HOH Au nanocrystals are 551, 542, 568, and 546 nm, respectively.

Catalytic Performance of Convex HOH Pd@Au Core–Shell Nanocrystals toward ECL. Luminol-H_2O_2 is one of the most important ECL systems with broad applications. The ECL reactions of luminol and H_2O_2 on Au electrodes are highly sensitive to surface properties.[30,31] At the cathode, H_2O_2 and O_2 molecules accept one electron to form $HO^•$ and $O_2^{•-}$ radicals on the nanocrystal surface. $HO^•$ radicals then oxidize luminol anions to luminol radicals. Luminol radicals and superoxide radicals $O_2^{•-}$ form an unstable complex (endoperoxide species) which evolves into excited 3-aminophthalate dianion by releasing a N_2 molecule. Excited dianions subsequently return to their ground state by emitting photons at 425 nm. Figure 5A demonstrates that 81 nm convex HOH Pd@Au core–shell nanocrystals deposited on glassy carbon electrodes can catalyze the ECL reactions of luminol and H_2O_2 with excelling activities. The ECL signal of convex HOH nanocrystals at 0.002 V was 50% stronger than that of concave trisoctahedra and 11 times stronger than that of truncated octahedra. The remarkably enhanced ECL activity of convex HOH Pd@Au core–shell nanocrystals is attributed to the abundance of atoms at kink and

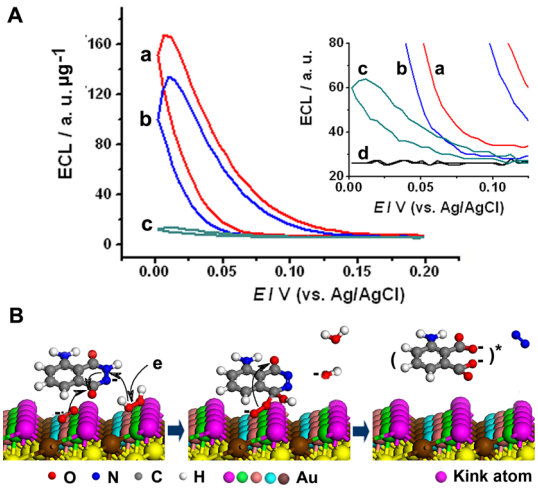

Figure 5. (A) ECL–potential curves of luminol/H_2O_2 system on (a) convex HOH, (b) concave trisoctahedral, and (c) truncated octahedral Pd@Au core–shell nanocrystal-modified glassy carbon electrodes, and (d) bare glassy carbon electrode. Inset: Corresponding enlarged curves in the 0–0.125 V range. Reaction conditions: luminol, 100 μM; H_2O_2, 100 μM; phosphate buffer solution, pH 7.4, 100 mM. (B) ECL reaction mechanism catalyzed by the {431} high-index facets of Au. The arrows point to the directions of electron transfers. Au atoms of different colors represent different atomic layers.

step sites on {431} high-index facets (Figure 5B).[32] First, the atomic vacancies from the high-index facets can provide active sites for the generation of oxygenated radicals ($HO^•$, $O_2^{•-}$), thus promoting electron transfer between hydroxyl radicals and luminol anions.[32,33] Second, unsaturated atoms at kink and step sites may stabilize intermediates including endoperoxide species, which facilitates the oxidation of luminol radicals by superoxide radicals.[30,34,35] Third, the coordination number of kink atoms on {431} high-index facets is lower than that of step atoms (Figure S8), resulting in the higher catalytic activity of {431} high-index facets over {331} high-index facets with only step atoms.[21] The ECL catalytic properties of convex HOH Pd@Au core–shell nanocrystals depend on the sizes and improve as the sizes decrease (Figure S9). The convex HOH Au nanocrystals of 81 nm exhibit similar catalytic activities to Pd@Au core–shell counterparts, indicating that the catalytic activity depends on the surface structures of Au shells.[36] The convex HOH Pd@Au core–shell nanocrystals can preserve their original morphologies (Figure S10) and catalytic activities after 3 months (Figure S11). The outstanding stability and superior ECL catalytic properties of convex HOH Pd@Au core–shell nanocrystals make them promising candidates for ultrasensitive detection systems.[37−40]

CONCLUSIONS

Convex HOH Pd@Au core–shell nanocrystals with {431} high-index facets have been synthesized using a facile chemical reduction method through fast growth

kinetics and the use of CPC as capping agent. The convex HOH Pd@Au core–shell nanocrystals exhibit remarkably improved activities in the ECL reactions of luminol and H_2O_2 as a consequence of the abundant atoms in kink and step sites on {431} high-index facets. The proposed system is envisaged to provide an alternative strategy for the shape-controlled synthesis of nanocrystals with high-index facets and for future sensitivity-enhanced ECL processes and bioanalytical detection methods.

METHODS

Materials. $PdCl_2$, $HAuCl_4 \cdot 4H_2O$, and CPC were obtained from Sinopharm Chemical Reagent Co. Ltd. (Shanghai, China). CTAC (98.0%), cetyltrimethylammonium bromide (CTAB), and 3-aminophthalhydrazide (luminol, ≥98%) were purchased from Tianjin Guangfu Fine Chemical Research Institute (China), Fluka (Switzerland), and Aldrich, respectively. AA and hydrogen peroxide (30%) was obtained from Beijing Chemical Reagent Company. All the chemicals were of analytical grade and used without further purification. Doubly distilled water was used throughout the experiments. A 10 mM H_2PdCl_4 solution was prepared by dissolving 0.1773 g of $PdCl_2$ in 10 mL of 0.2 M HCl solution and further diluting to 100 mL with doubly distilled water.

Synthesis of 22 nm Cubic Pd Seeds. Cubic Pd seeds (22 nm) were synthesized with the previous method.[19] Briefly, a 500 μL aliquot of 10 mM H_2PdCl_4 solution was added to 9.42 mL of 12.5 mM CTAB aqueous solution heated at 95 °C under stirring. After 5 min, 80 μL of freshly prepared 100 mM AA aqueous solution was added, and the reaction was allowed to proceed for 20 min. Then, the 22 nm Pd nanocubes were washed for one time with 5 mM CPC aqueous solution and collected into 10 mL of 5 mM CPC aqueous solution and stored at 30 °C for future use.

Synthesis of 39 nm Near-Spherical Au Seeds. Near-spherical Au nanocrystals (39 nm) were synthesized with the previous method.[20,41,42] First, ~1.5 nm Au seeds were prepared by adding a 0.3 mL aliquot of 10 mM ice-cold $NaBH_4$ solution into 5 mL of 100 mM CTAB solution containing 0.25 mM $HAuCl_4$, followed by rapid inversion mixing for 2 min and stored at 30 °C for future use. Second, Au nanorods were prepared by adding 24 μL aliquot of the ~1.5 nm Au seed solution into 20 mL CTAB solution containing 5 μM $HAuCl_4$, 0.6 μM $AgNO_3$, and 8 μM AA at 30 °C. The solution was left undisturbed and aged for 2 h. The nanorods obtained were separated and washed with water once by centrifugation (12 000 rpm, 10 min) and redispersed in 20 mL of 10 mM CTAB solution at 40 °C containing 0.5 mM $HAuCl_4$ and 1.6 mM AA for second overgrowth. The mixture was allowed to react at 40 °C for 1 h. Third, the overgrown Au nanorods were separated by centrifugation (10 000 rpm, 10 min) and redispersed in 20 mL of 10 mM CTAB solution containing 0.2 mM $HAuCl_4$ at 40 °C to produce 39 nm near-spherical Au nanocrystals. The mixture was left undisturbed and aged for 12 h. Finally, the 39 nm near-spherical Au seed solution was washed twice with 5 mM CPC solution by centrifugation (10 000 rpm, 10 min) and dispersed in 20 mL of 5 mM CPC solution and stored at 30 °C for further use.

Synthesis of Convex HOH Pd@Au Core–Shell Nanocrystals. In a typical synthesis, 5 mL of 5 mM CPC aqueous solution was kept at 30 °C for 10 min. Then, a 10 μL aliquot of 22 nm cubic Pd seed aqueous solution, 144 μL aliquot of 100 mM freshly prepared AA, and 300 μL aliquot of 10 mM $HAuCl_4$ were added successively into CPC solution. The reaction solution became yellow and then colorless instantly. The colorless solution gradually became dark pink in 1 min and finally orange pink in 9 min. The resultant nanocrystal solutions were centrifuged at 6000 rpm for 3 min. The precipitate was washed with warm water for further characterization.

ECL Catalysis of Pd@Au Core–Shell Nanocrystals. The {431}-faceted convex HOH, {331}-faceted, and truncated octahedral Pd@Au core–shell nanocrystals of 81 nm were used to catalyze the ECL reaction of luminol and H_2O_2. Eight microliters of colloidal nanocrystal solution (nanoparticles with 81 nm, 4.72 μg) was dropped onto fresh glassy carbon electrodes (diameter, 3 mm) and dried at room temperature to make working electrodes. Then the nanocrystal-modified working electrodes were cleaned with air plasma for 1 min to remove the remaining surfactants adsorbed on the nanocrystal surfaces.[43] As shown in Figure S12, the nanocrystal morphologies are maintained after plasma cleaning. Cyclic voltammetry (CV) experiments and ECL measurements were carried out in a conventional three-electrode cell with an MPI-A capillary electrophoresis ECL detector (Xi'an Remex Electronics Co. Ltd., Xi'an, China) at room temperature (photomultiplier tube, −600 V). The auxiliary electrode and the reference electrode are a thin gold grid and a Ag/AgCl electrode (saturated KCl), respectively. Before the ECL catalysis experiments, the nanocrystal-modified working electrodes were electrochemically cleaned in 0.5 M H_2SO_4 solutions with CV techniques between −0.4 and 1.6 V (*vs* Ag/AgCl) for 10 cycles.

Instruments. SEM images were taken using an FEI XL30 ESEM FEG scanning electron microscope operated at 25 kV. TEM images were obtained using a FEI Tecnai G2 F20 microscope operated at 200 kV. HAADF-STEM images and elemental mapping images were obtained using a FEI Tecnai G2 F20 S-TWIN microscope operated at 200 kV. X-ray photoelectron spectroscopy spectra were taken on Thermo ESCALAB 250. UV–vis extinction spectra were obtained using WFZ UV-2802PC spectrometer. Harrick plasma cleaner PDC-32G was used to clean the nanocrystal surfaces with the power of 720 V/10 mA DC using air as the pumping gas.

Conflict of Interest: The authors declare no competing financial interest.

Acknowledgment. This work is kindly supported by the National Natural Science Foundation of China (No. 21175126), Changchun Institute of Applied Chemistry, and Chinese Academy of Sciences.

Supporting Information Available: SEM images, TEM images, XPS, extinction spectra, atomic models, ECL–potential curves, and additional data. This material is available free of charge *via* the Internet at http://pubs.acs.org.

REFERENCES AND NOTES

1. Zhang, L.; Niu, W.; Xu, G. Synthesis and Applications of Noble Metal Nanocrystals with High-Energy Facets. *Nano Today* **2012**, *7*, 586–605.
2. Quan, Z.; Wang, Y.; Fang, J. High-Index Faceted Noble Metal Nanocrystals. *Acc. Chem. Res.* **2013**, *46*, 191–202.
3. Kim, T.; Hyeon, T. Applications of Inorganic Nanoparticles as Therapeutic Agents. *Nanotechnology* **2014**, *25*, 012001.
4. Maoz, B. M.; Chaikin, Y.; Tesler, A. B.; Bar Elli, O.; Fan, Z.; Govorov, A. O.; Markovich, G. Amplification of Chiroptical Activity of Chiral Biomolecules by Surface Plasmons. *Nano Lett.* **2013**, *13*, 1203–1209.
5. Lee, Y. W.; Kim, D.; Hong, J. W.; Kang, S. W.; Lee, S. B.; Han, S. W. Kinetically Controlled Growth of Polyhedral Bimetallic Alloy Nanocrystals Exclusively Bound by High-Index Facets: AuPd Hexoctahedra. *Small* **2013**, *9*, 660–665.
6. Zhang, H.; Jin, M.; Xia, Y. Noble-Metal Nanocrystals with Concave Surfaces: Synthesis and Applications. *Angew. Chem., Int. Ed.* **2012**, *51*, 7656–7673.
7. Lin, H. X.; Lei, Z. C.; Jiang, Z. Y.; Hou, C. P.; Liu, D. Y.; Xu, M. M.; Tian, Z. Q.; Xie, Z. X. Supersaturation-Dependent Surface Structure Evolution: From Ionic, Molecular to Metallic Micro/Nanocrystals. *J. Am. Chem. Soc.* **2013**, *135*, 9311–9314.

8. Hong, J. W.; Lee, S. U.; Lee, Y. W.; Han, S. W. Hexoctahedral Au Nanocrystals with High-Index Facets and Their Optical and Surface-Enhanced Raman Scattering Properties. *J. Am. Chem. Soc.* **2012**, *134*, 4565–4568.
9. Wang, F.; Li, C.; Sun, L. D.; Wu, H.; Ming, T.; Wang, J.; Yu, J. C.; Yan, C. H. Heteroepitaxial Growth of High-Index-Faceted Palladium Nanoshells and Their Catalytic Performance. *J. Am. Chem. Soc.* **2011**, *133*, 1106–1111.
10. Ma, Y.; Kuang, Q.; Jiang, Z.; Xie, Z.; Huang, R.; Zheng, L. Synthesis of Trisoctahedral Gold Nanocrystals with Exposed High-Index Facets by a Facile Chemical Method. *Angew. Chem., Int. Ed.* **2008**, *47*, 8901–8904.
11. Personick, M. L.; Langille, M. R.; Wu, J.; Mirkin, C. A. Synthesis of Gold Hexagonal Bipyramids Directed by Planar-Twinned Silver Triangular Nanoprisms. *J. Am. Chem. Soc.* **2013**, *135*, 3800–3803.
12. Tao, A. R.; Habas, S.; Yang, P. Shape Control of Colloidal Metal Nanocrystals. *Small* **2008**, *4*, 310–325.
13. Zhang, J.; Hou, C.; Huang, H.; Zhang, L.; Jiang, Z.; Chen, G.; Jia, Y.; Kuang, Q.; Xie, Z.; Zheng, L. Surfactant-Concentration-Dependent Shape Evolution of AuPd Alloy Nanocrystals from Rhombic Dodecahedron to Trisoctahedron and Hexoctahedron. *Small* **2013**, *9*, 538–544.
14. Zhang, L.; Zhang, J.; Kuang, Q.; Xie, S.; Jiang, Z.; Xie, Z.; Zheng, L. Cu^{2+}-Assisted Synthesis of Hexoctahedral Au–Pd Alloy Nanocrystals with High-Index Facets. *J. Am. Chem. Soc.* **2011**, *133*, 17114–17117.
15. Kim, D.; Lee, Y. W.; Lee, S. B.; Han, S. W. Convex Polyhedral Au@Pd Core–Shell Nanocrystals with High-Index Facets. *Angew. Chem., Int. Ed.* **2012**, *51*, 159–163.
16. Personick, M. L.; Mirkin, C. A. Making Sense of the Mayhem behind Shape Control in the Synthesis of Gold Nanoparticles. *J. Am. Chem. Soc.* **2013**, *135*, 18238–18247.
17. Xia, Y.; Xiong, Y.; Lim, B.; Skrabalak, S. E. Shape-Controlled Synthesis of Metal Nanocrystals Simple Chemistry Meets Complex Physics? *Angew. Chem., Int. Ed.* **2009**, *48*, 60–103.
18. Yu, Y.; Zhang, Q.; Liu, B.; Lee, J. Y. Synthesis of Nanocrystals with Variable High-Index Pd Facets through the Controlled Heteroepitaxial Growth of Trisoctahedral Au Templates. *J. Am. Chem. Soc.* **2010**, *132*, 18258–18265.
19. Niu, W.; Li, Z. Y.; Shi, L.; Liu, X.; Li, H.; Han, S.; Chen, J.; Xu, G. Seed-Mediated Growth of Nearly Monodisperse Palladium Nanocubes with Controllable Sizes. *Cryst. Growth Des.* **2008**, *8*, 4440–4444.
20. Niu, W.; Zheng, S.; Wang, D.; Liu, X.; Li, H.; Han, S.; Chen, J.; Tang, Z.; Xu, G. Selective Synthesis of Single-Crystalline Rhombic Dodecahedral, Octahedral, and Cubic Gold Nanocrystals. *J. Am. Chem. Soc.* **2008**, *131*, 697–703.
21. Cai, L.; Lu, G.; Zhan, W.; Guo, Y.; Guo, Y.; Yang, Q.; Zhang, Z. The Effect of Preparation Method on the Activities of Pd-Fe-Ox/Al_2O_3 Catalysts for CO Oxidation. *J. Mater. Sci.* **2011**, *46*, 5639–5644.
22. Qian, L.; Zhou, L.; Too, H. P.; Chow, G. M. Gold Decorated $NaYF_4$:Yb,Er/$NaYF_4$/Silica (Core/Shell/Shell) Upconversion Nanoparticles for Photothermal Destruction of BE(2)-C Neuroblastoma Cells. *J. Nanopart. Res.* **2011**, *13*, 499–510.
23. Zhou, Z. Y.; Tian, N.; Huang, Z. Z.; Chen, D. J.; Sun, S. G. Nanoparticle Catalysts with High Energy Surfaces and Enhanced Activity Synthesized by Electrochemical Method. *Faraday Discuss.* **2009**, *140*, 81–92.
24. Sau, T. K.; Murphy, C. J. Room Temperature, High-Yield Synthesis of Multiple Shapes of Gold Nanoparticles in Aqueous Solution. *J. Am. Chem. Soc.* **2004**, *126*, 8648–8649.
25. Bealing, C. R.; Baumgardner, W. J.; Choi, J. J.; Hanrath, T.; Hennig, R. G. Predicting Nanocrystal Shape through Consideration of Surface–Ligand Interactions. *ACS Nano* **2012**, *6*, 2118–2127.
26. Niu, W.; Zhang, L.; Xu, G. Shape-Controlled Synthesis of Single-Crystalline Palladium Nanocrystals. *ACS Nano* **2010**, *4*, 1987–1996.
27. Ding, Y.; Fan, F.; Tian, Z.; Wang, Z. L. Atomic Structure of Au–Pd Bimetallic Alloyed Nanoparticles. *J. Am. Chem. Soc.* **2010**, *132*, 12480–12486.
28. Wang, F.; Sun, L. D.; Feng, W.; Chen, H.; Yeung, M. H.; Wang, J.; Yan, C. H. Heteroepitaxial Growth of Core–Shell and Core–Multishell Nanocrystals Composed of Palladium and Gold. *Small* **2010**, *6*, 2566–2575.
29. Lee, Y. W.; Kim, M.; Kim, Z. H.; Han, S. W. One-Step Synthesis of Au@Pd Core–Shell Nanooctahedron. *J. Am. Chem. Soc.* **2009**, *131*, 17036–17037.
30. Cui, H.; Xu, Y.; Zhang, Z. F. Multichannel Electrochemiluminescence of Luminol in Neutral and Alkaline Aqueous Solutions on a Gold Nanoparticle Self-Assembled Electrode. *Anal. Chem.* **2004**, *76*, 4002–4010.
31. Zhang, L.; Niu, W.; Gao, W.; Majeed, S.; Liu, Z.; Zhao, J.; Anjum, S.; Xu, G. Synthesis and Electrocatalytic Properties of Tetrahexahedral, Polyhedral, and Branched Pd@Au Core–Shell Nanocrystals. *Chem. Commun.* **2013**, *49*, 8836–8838.
32. Tian, N.; Zhou, Z. Y.; Sun, S. G.; Ding, Y.; Wang, Z. L. Synthesis of Tetrahexahedral Platinum Nanocrystals with High-Index Facets and High Electro-oxidation Activity. *Science* **2007**, *316*, 732–735.
33. Lu, C. L.; Prasad, K. S.; Wu, H. L.; Ho, J. A. A.; Huang, M. H. Au Nanocube-Directed Fabrication of Au–Pd Core–Shell Nanocrystals with Tetrahexahedral, Concave Octahedral, and Octahedral Structures and Their Electrocatalytic Activity. *J. Am. Chem. Soc.* **2010**, *132*, 14546–14553.
34. Zhang, L.; Niu, W.; Zhao, J.; Zhu, S.; Yuan, Y.; Yuan, T.; Hu, L.; Xu, G. Pd@Au Core–Shell Nanocrystals with Concave Cubic Shapes: Kinetically Controlled Synthesis and Electrocatalytic Properties. *Faraday Discuss.* **2013**, *164*, 175–188.
35. Zhang, Z. F.; Cui, H.; Lai, C. Z.; Liu, L. J. Gold Nanoparticle-Catalyzed Luminol Chemiluminescence and Its Analytical Applications. *Anal. Chem.* **2005**, *77*, 3324–3329.
36. Cui, C. H.; Yu, J. W.; Li, H. H.; Gao, M. R.; Liang, H. W.; Yu, S. H. Remarkable Enhancement of Electrocatalytic Activity by Tuning the Interface of Pd–Au Bimetallic Nanoparticle Tubes. *ACS Nano* **2011**, *5*, 4211–4218.
37. Kato, D.; Sumimoto, M.; Ueda, A.; Hirono, S.; Niwa, O. Evaluation of Electrokinetic Parameters for All DNA Bases with Sputter Deposited Nanocarbon Film Electrode. *Anal. Chem.* **2012**, *84*, 10607–10613.
38. Liu, S. Q.; Zheng, Z. Z.; Li, X. Y. Advances in Pesticide Biosensors: Current Status, Challenges, and Future Perspectives. *Anal. Bioanal. Chem.* **2013**, *405*, 63–90.
39. Miao, W. Electrogenerated Chemiluminescence and Its Biorelated Applications. *Chem. Rev.* **2008**, *108*, 2506–2553.
40. Richter, M. M. Electrochemiluminescence (ECL). *Chem. Rev.* **2004**, *104*, 3003–3036.
41. Keul, H. A.; Möller, M.; Bockstaller, M. R. Structural Evolution of Gold Nanorods during Controlled Secondary Growth. *Langmuir* **2007**, *23*, 10307–10315.
42. Nikoobakht, B.; El-Sayed, M. A. Preparation and Growth Mechanism of Gold Nanorods (NRs) Using Seed-Mediated Growth Method. *Chem. Mater.* **2003**, *15*, 1957–1962.
43. Petasch, W.; Kegel, B.; Schmid, H.; Lendenmann, K.; Keller, H. U. Low-Pressure Plasma Cleaning: A Process for Precision Cleaning Applications. *Surf. Coat. Technol.* **1997**, *97*, 176–181.